LETTERS

Rapid planetesimal formation in turbulent circumstellar disks

Anders Johansen[1], Jeffrey S. Oishi[2,3], Mordecai-Mark Mac Low[1,2], Hubert Klahr[1], Thomas Henning[1] & Andrew Youdin[4]

During the initial stages of planet formation in circumstellar gas disks, dust grains collide and build up larger and larger bodies[1]. How this process continues from metre-sized boulders to kilometre-scale planetesimals is a major unsolved problem[2]: boulders are expected to stick together poorly[3], and to spiral into the protostar in a few hundred orbits owing to a 'headwind' from the slower rotating gas[4]. Gravitational collapse of the solid component has been suggested to overcome this barrier[1,5,6]. But even low levels of turbulence will inhibit sedimentation of solids to a sufficiently dense midplane layer[2,7], and turbulence must be present to explain observed gas accretion in protostellar disks[8]. Here we report that boulders can undergo efficient gravitational collapse in locally overdense regions in the midplane of the disk. The boulders concentrate initially in transient high pressure regions in the turbulent gas[9], and these concentrations are augmented a further order of magnitude by a streaming instability[10–12] driven by the relative flow of gas and solids. We find that gravitationally bound clusters form with masses comparable to dwarf planets and containing a distribution of boulder sizes. Gravitational collapse happens much faster than radial drift, offering a possible path to planetesimal formation in accreting circumstellar disks.

Planet formation models typically treat turbulence as a diffusive process that opposes the gravitational sedimentation of solids to a high density midplane layer in circumstellar disks[7,13]. Recent models of solids moving in turbulent gas reveal that the turbulent motions not only mix them, but also concentrate metre-sized boulders in the transient gas overdensities[9] formed in magnetorotational turbulence[14], in giant gaseous vortices[15,16], and in spiral arms of self-gravitating disks[17]. Short-lived eddies at the dissipation scale of forced turbulence concentrate smaller millimetre-sized solids[18].

Some simulations mentioned above[9,11,12] were performed with the Pencil Code, which solves the magnetohydrodynamic equations on a three-dimensional grid for a gas that interacts through drag forces with boulders. Boulders are represented as superparticles with independent positions and velocities, each having the mass of a huge number of boulders but the aerodynamic behaviour of a single boulder. We have now further developed the Pencil Code to include a fully parallel solver for the gravitational potential of the particles (see Supplementary Information). The particle density is mapped on the grid using the 'triangular shaped cloud' assignment scheme[19] and the gravitational potential of the solids is found using a fast Fourier transform method[20]. This allows us, for the first time to our knowledge, to simulate the dynamics of self-gravitating solid particles in magnetized, three-dimensional turbulence.

We model a co-rotating, local box with linearized keplerian shear that straddles the protoplanetary disk midplane and orbits the young star at a fixed distance. Periodic boundary conditions are applied. An isothermal equation of state is used for the gas, whereas the induction equation is solved under the ideal magnetohydrodynamic assumption of high conductivity. Magnetorotational instability[14] drives turbulence in keplerian disks with sufficient ionization[21], producing in our unstratified models turbulence with Mach number $\mathrm{Ma} \approx 0.05$ and viscosity $\alpha \approx 10^{-3}$, a realistic value to explain observed accretion rates[8]. The ionization fraction in the dense midplanes of protoplanetary disks may be insufficient for the gas to couple with the magnetic field to drive magnetorotational instability[21]. In the Supplementary Information we therefore describe unmagnetized models as well.

Solid objects orbit the protostar with keplerian velocity v_K in the absence of gas drag. A radial pressure gradient partly supports the gas, however, so it orbits at sub-keplerian velocity v_g, with $\Delta v \equiv v_\mathrm{g} - v_\mathrm{K} < 0$. As a result, large (approximately metre-sized) solid objects are exposed to a strong headwind that causes them to drift radially inwards[4] with a maximum drift velocity Δv. They also 'feel' gas drag as they fall towards the disk midplane in the effective gravity field of the star. A sedimentary midplane layer forms, with a width determined by a balance between settling and turbulent diffusion[7,13].

We present three types of models: (1) without self-gravity, with 128^3 zones and 2×10^6 particles, run for 100 orbits, to study the interplay between the streaming instability[10] and concentration by transient high pressures; (2) with self-gravity and boulder collisions, with 256^3 zones and 8×10^6 particles run for 27 orbits, to study gravitational collapse; and (3) models with self-gravity but no magnetorotational turbulence (presented in the Supplementary Information). Magnetorotational turbulence is given 10 orbits to reach steady state before we turn on drag force and vertical gravity, to avoid any influence of the initial conditions on the sedimented midplane layer. We fix the global solids-to-gas bulk density ratio at the canonical galactic value of $\varepsilon_0 = 0.01$, but two values of the radial drift are considered: low drift, with $\Delta v = -0.02 c_\mathrm{s}$, where c_s is the isothermal sound speed, and moderate drift, with $\Delta v = -0.05 c_\mathrm{s}$, depending on the assumed radial pressure support (values up to $\Delta v = -(0.2\text{–}0.5) c_\mathrm{s}$ are possible[13], but are not considered here).

For the simulations without self-gravity, we consider a fixed particle size parameterized by the dimensionless friction time $\Omega_\mathrm{K} \tau_\mathrm{f} = 1.0$, where Ω_K is the local keplerian rotation frequency and τ_f is the timescale over which gas and solids reach equal velocity. At an orbital distance $r = 5$ AU, this corresponds to boulders of approximately one metre in diameter. Figure 1 shows the space–time topography of the sedimented midplane layer. The streaming instability increases the density of boulders in regions where they have already

[1]Max-Planck-Institut für Astronomie, Königstuhl 17, D-69117 Heidelberg, Germany. [2]Department of Astrophysics, American Museum of Natural History, 79th Street at Central Park West, New York, New York 10024-5192, USA. [3]Department of Astronomy, University of Virginia, Charlottesville, Virginia 22904, USA. [4]Canadian Institute for Theoretical Astrophysics, University of Toronto, 60 St George Street, Toronto, Ontario M5S 3H8, Canada.

been concentrated by transient high pressures[9]. Increasing radial pressure support, by changing $\Delta v = -0.02c_s$ to $-0.05c_s$, reduces the concentration (see Fig. 1 legend for explanation), although the local solids-to-gas density ratio still reaches 200.

Gravitational collapse of discrete solid objects produces virialized clusters unable to contract further[22] in the absence of mechanisms to dynamically cool the cluster—that is, to reduce the local r.m.s. speed. Two processes that we consider can be important: drag force cooling and collisional cooling. Drag force cooling occurs because part of the kinetic energy exchanged between the particles and the gas is dissipated. Collisional cooling is produced by the highly inelastic collisions between boulders, transferring kinetic energy to heat and deformation. Collisional cooling occurs generally in simulations of resolved collisions in planetary rings[23]. In the Supplementary Information we describe how we treat collisional cooling numerically in the self-gravitating simulations by damping the r.m.s. speed of the particles in each grid cell on a collisional timescale. We have found that in the absence of collisional cooling, gravitational collapse still proceeds if the total surface density (of solids and gas) is augmented by 50%. Collisional cooling is thus not a prerequisite of the collapse, but does allow it to occur in somewhat less massive disks. We ignore all other effects of the collisions, such as coagulation and collisional fragmentation. Collisional cooling and self-gravity are turned on after 20 orbits in the self-gravitating simulations.

Our chosen scale-height-to-radius ratio of $H/r = 0.04$ gives a gas temperature of $T = 80$ K at an orbital radius of $r = 5$ AU. For the 256^3 self-gravitating run, we choose the uniform gas volume density to be consistent with the midplane of a disk with surface density of $\Sigma_{gas} = 300\,g\,cm^{-2}$. This corresponds to approximately twice the minimum-mass solar nebula at 5 AU from the (proto-)Sun. An alternative theory for giant planet formation, the disk instability hypothesis[24,25], requires column densities at least 20 times higher than the minimum-mass solar nebula for gravitational fragmentation of the gaseous component of the disk to occur.

We have examined the numerical convergence of our models with resolutions ranging from 64^3 to 256^3 zones (see Supplementary Information). The peak particle density on the grid increases with increasing resolution, because of less smoothing in the particle-mesh scheme at higher resolution, resulting in a decrease in the column density threshold for gravitational collapse. Although we have not yet achieved full convergence, our results seem to provide good upper limits to the column density for which collapse can occur. For the self-gravitating simulation, we consider boulders with friction times distributed among $\Omega_K\tau_f = 0.25, 0.50, 0.75, 1.00$. At $r = 5$ AU in our chosen disk model, these correspond to radii of 15–60 cm. Consideration of multiple boulder sizes is vital, as differential aerodynamic behaviour could inhibit gravitational instabilities[26]. The size range covers roughly half of the two orders of magnitude in particle

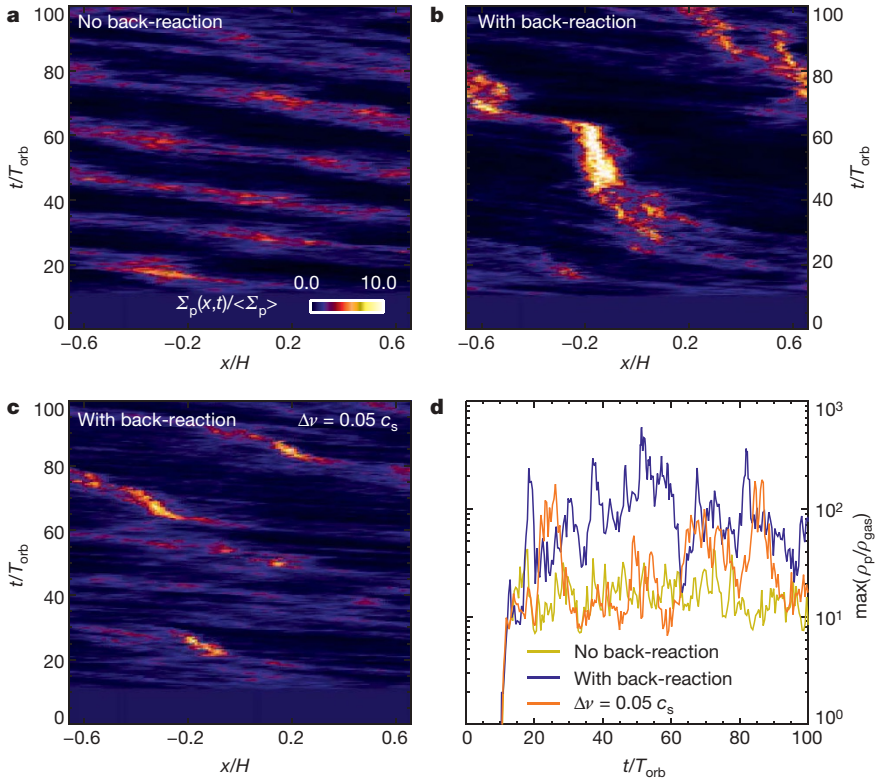

Figure 1 | Topography of the sedimented particle layer in models without self-gravity or collisional cooling. **a**, The azimuthally averaged vertical column density Σ_p of metre-sized boulders (with $\Omega_K\tau_f = 1$) as a function of radial coordinate x (in units of disk scale heights H) and time t (in orbits T_{orb}), in a model where the particles feel gas drag, but the gas does not feel drag from the particles. Radial drift is evident from the tilted bands (particles crossing the inner boundary reappear at the outer). Transient regions of mildly increased gas pressure temporarily concentrate boulders. The gas orbits slightly more slowly on the outer edge of these high pressure regions and slightly faster on the inner edge, resulting in a differential headwind that forces boulders towards the centres of these high-pressure regions[9,30]. **b**, Including the back-reaction drag force from the particles on the gas allows for the development of the streaming instability, seeded by the existing radial density enhancements. The streaming instability occurs where the collective drag force of the solids forces the gas to locally move with an orbital speed that is closer to keplerian, reducing the gaseous headwind that otherwise causes boulders to drift radially. Solids then drift into already overdense regions from further out, causing runaway growth in the local bulk density of solids. **c**, The column density when the radial pressure support is changed from $\Delta v = -0.02c_s$ to $-0.05c_s$. Radial density enhancements become narrower and shorter-lived owing to downstream erosion of the overdensities by the stronger radial drift. **d**, The maximum particle density ρ_p on the grid (in units of the gas density ρ_{gas}) as a function of time. The average solids-to-gas ratio in the midplane is 0.5, whereas the maximum reaches well over ten times higher values in transient high pressure regions (yellow) and several hundred times higher values when the streaming instability is active (orange and blue).

radius produced by coagulation of microscopic grains[27]. Smaller particles are ignored, as they are unlikely to separate from the gas and participate in gravitational collapse. In the case of widespread collisional fragmentation, for example, in the warmer terrestrial planet formation region, up to 80% of the solid material may be bound in small fragments[27,28], in which case we must implicitly assume an augmentation in solids-to-gas ratio of up to 5 to reach our assumed amount of boulders.

In our self-gravitating model we set $\Delta v = -0.02 c_s$, but show in the Supplementary Information that gravitationally bound clusters also form for $\Delta v = -0.05 c_s$, with a factor of two increase in column density threshold. The Supplementary Information also documents that typical boulder collisions happen at speeds below the expected destruction threshold[3]. We warn, however, that material properties, and thus destruction thresholds, of the boulders are poorly known. Higher resolution studies, and an improved analytical theory of collision speeds that takes into account epicyclic motion, will be needed to determine whether collision speeds have converged; this is because we find an unexplained factor 3 difference for $\Omega_K \tau_f = 1$ particles between typical relative speeds within cells ($\sim 5\,\mathrm{m\,s^{-1}}$) and the expected collision speed of well-mixed particles.

The development of gravitational instability in the 256^3 run is shown in Fig. 2. The four different boulder sizes have already accumulated in the same regions (see the block of four joined panels) before self-gravity is turned on, demonstrating that differential drift does not prevent density enhancement by streaming instability. Gravitationally bound boulder clusters form, with a Hill radius—within which the gravity of the cluster dominates over tidal forces from the central star—that increases steadily with time (insets) as the clusters accrete boulders from the surrounding flow.

We show in Fig. 3 the peak density and the mass of the most massive gravitationally bound cluster as a function of time. The cluster consists of particles of all four sizes, demonstrating that different boulder sizes can indeed take part in the same gravitational collapse, despite their different aerodynamical properties and drift behaviour. At the end of the simulation, the most massive cluster contains 3.5 times the mass of the dwarf planet Ceres. The cluster mass agrees roughly with standard estimates from linear gravitational instability[5], when applied at $r = 5$ AU to the locally enhanced column densities (see Supplementary Information).

Models lacking magnetic fields, and thus magnetorotational turbulence, are described in the Supplementary Information. Here sedimentation occurs unhindered until the onset of Kelvin–Helmholtz instabilities driven by the vertical shear of gas velocity above the midplane boulder layer. Strong boulder density enhancements in the mid-plane layer nevertheless still form, although for moderate drift an increase of the solids-to-gas ratio from 0.01 to 0.03 was needed to obtain strong clumping. (Such an increase may

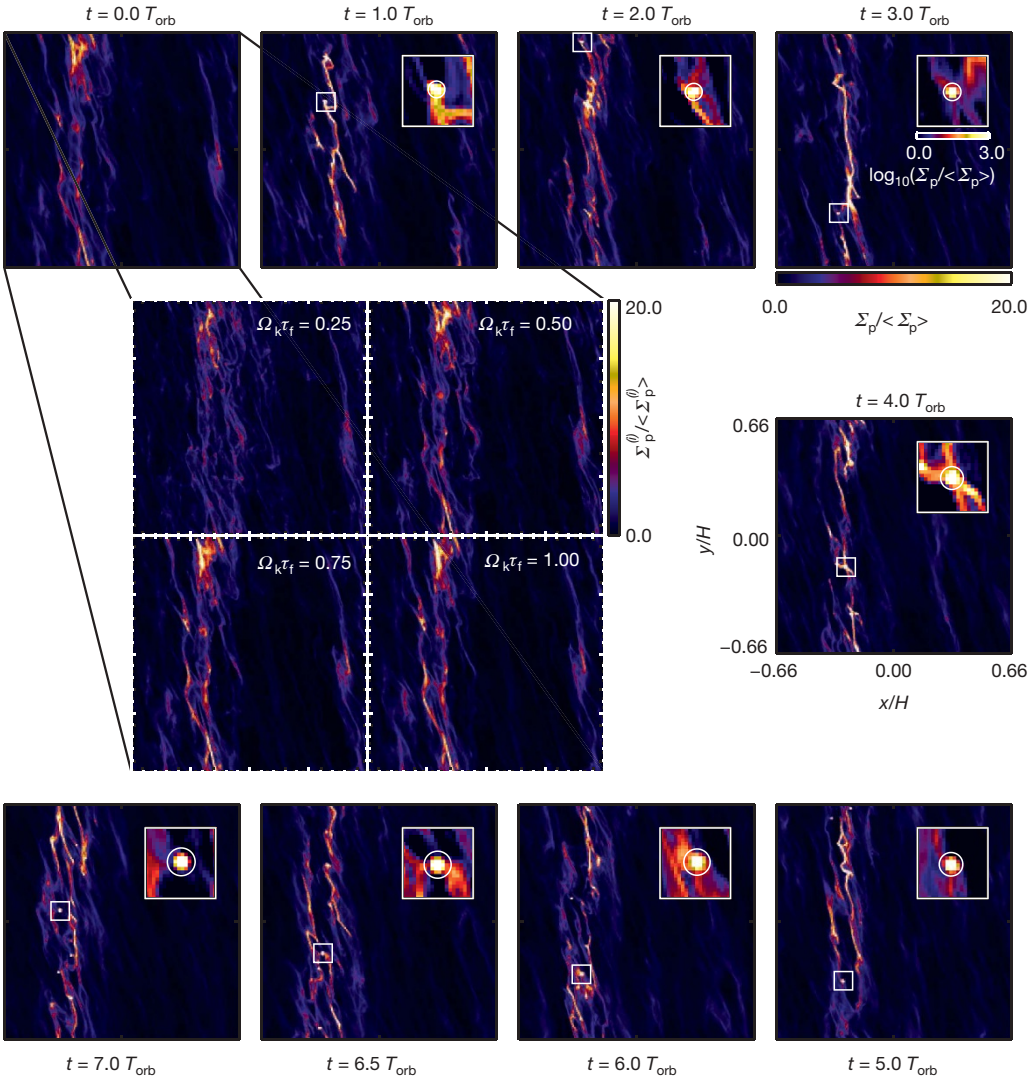

Figure 2 | Time series of the collapse of overdense seeds into gravitationally bound boulder clusters. The central block of four panels shows the column densities of the four different sizes of boulders (in units of the mean column density of each size) plotted independently at a time just before self-gravity is turned on. All four particle sizes have concentrated at similar locations, an important prerequisite for the subsequent gravitational collapse. The surrounding panels show a time series of total column density of solids, in the radial–azimuthal (x–y) plane of the disk, summed over all particle sizes, starting from the upper left and progressing clockwise. Values are normalized to the average value across the grid (see colour bars in upper right panel). Times are given in orbital times T_{orb} after self-gravity is turned on. Inset in each panel is an enlargement of a square region (indicated in the main panel) centred around the Hill sphere of the most massive cluster in the simulation, represented by the white circle. These insets show the log of the column density ratio (see colour bar in upper right panel) to capture the extreme values reached. Overdense bands initially contract radially, forming thin filaments with densities high enough for a full non-axisymmetric collapse into gravitationally bound clumps to take place. As time progresses, the Hill sphere increases in radius as the clusters grow in mass by accreting boulders from the turbulent flow (see Supplementary Video for an animation of this simulation).

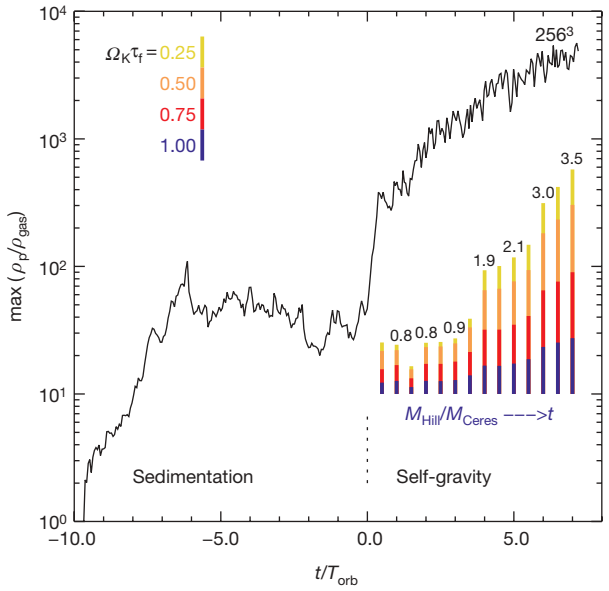

Figure 3 | Mass accretion onto a gravitationally bound cluster. Main plot, the maximum bulk density of solids ρ_p as a function of time, normalized by the average gas density ρ_{gas}. Drag force and vertical gravity are turned on at $t = -10$, whereas self-gravity and collisional cooling are turned on at $t = 0$. The density increases monotonically after the onset of self-gravity because gravitationally bound clusters of boulders form in the mid-plane. After only seven orbits, peak densities in these clusters approach $10^4\rho_{gas}$ or a million times the average boulder density in the disk. Bottom right inset, coloured bars show (by their height, given on top) the mass contained within the most massive Hill sphere in the box, in units of the mass of the 970-km-radius dwarf planet Ceres ($M_{Ceres} = 9.5 \times 10^{23}$ g). The most massive cluster accretes about $0.5M_{Ceres}$ per orbit (the entire box contains a total boulder mass of $50M_{Ceres}$). The cluster consists of approximately equal fractions of the three larger boulder sizes (see colour bar inset at top left). The smallest size, with $\Omega_K\tau_f = 0.25$, is initially underrepresented with a fraction of only 15% because of the stronger aerodynamic coupling of those particles to the gas, but the fraction of small particles increases with time as the cluster grows massive enough to attract smaller particles as well. The mean free path inside the bound clusters is shorter than the size of the cluster, so any fragments formed in catastrophic collisions between the boulders will be swept up by the remaining boulders before being able to escape the cluster (see Supplementary Information).

perhaps be possible owing to radial variation in boulder drift speeds[6] or photoevaporation of the gas[29].) Magnetorotational turbulence thus has a positive effect on the mid-plane layer's ability to gravitationally collapse, although collapse can also occur without it.

The Supplementary Information also includes a model with an adiabatic equation of state and explicit gas heating due to energy dissipated by drag and inelastic collisions. We find that gas heating does not prevent collapse. The maximum temperature reached is not even high enough to melt ice, although that may change with the formation of massive bodies with escape velocity near the sound speed.

Our proposed path to planetesimal formation depends crucially on the existence of a dense sedimentary layer of boulders. Future investigations should focus on the formation and survival of such layers in the light of processes like coagulation, collisional fragmentation and erosion[28]. Especially important are higher resolution studies of collision speeds, and an improved analytical theory of collisions that includes the epicyclic motion of particles.

Received 19 December 2006; accepted 5 July 2007.

1. Safronov, V. S. *Evolution of the Protoplanetary Cloud and Formation of Earth and the Planets* (NASA Tech. Transl. F-677, Jerusalem, 1972); translation of *Evoliutsiia Doplanetnogo Oblaka* (Nauka, Moscow, 1969).
2. Dominik, C., Blum, J., Cuzzi, J. N. & Wurm, G. in *Protostars and Planets V* (eds Reipurth, B., Jewitt, D. & Keil, K.) 783–800 (Univ. Arizona Press, Tucson, 2007).
3. Benz, W. Low velocity collisions and the growth of planetesimals. *Space Sci. Rev.* **92,** 279–294 (2000).
4. Weidenschilling, S. J. Aerodynamics of solid bodies in the solar nebula. *Mon. Not. R. Astron. Soc.* **180,** 57–70 (1977).
5. Goldreich, P. & Ward, W. R. The formation of planetesimals. *Astrophys. J.* **183,** 1051–1062 (1973).
6. Youdin, A. N. & Shu, F. H. Planetesimal formation by gravitational instability. *Astrophys. J.* **580,** 494–505 (2002).
7. Weidenschilling, S. J. & Cuzzi, J. N. in *Protostars and Planets III* (eds Levy, E. H. & Lunine, J. I.) 1031–1060 (Univ. Arizona Press, Tucson, 1993).
8. Hartmann, L. *Accretion Processes in Star Formation* (Cambridge Astrophysics Series No. 32, Cambridge Univ. Press, Cambridge, UK, 1998).
9. Johansen, A., Klahr, H. & Henning, T. Gravoturbulent formation of planetesimals. *Astrophys. J.* **636,** 1121–1134 (2006).
10. Youdin, A. N. & Goodman, J. Streaming instabilities in protoplanetary disks. *Astrophys. J.* **620,** 459–469 (2005).
11. Johansen, A., Henning, T. & Klahr, H. Dust sedimentation and self-sustained Kelvin-Helmholtz turbulence in protoplanetary disk midplanes. *Astrophys. J.* **643,** 1219–1232 (2006).
12. Johansen, A. & Youdin, A. Protoplanetary disk turbulence driven by the streaming instability: Nonlinear saturation and particle concentration. *Astrophys. J.* **662,** 627–641 (2007).
13. Cuzzi, J. N., Dobrovolskis, A. R. & Champney, J. M. Particle-gas dynamics in the midplane of a protoplanetary nebula. *Icarus* **106,** 102–134 (1993).
14. Balbus, S. A. & Hawley, J. F. Instability, turbulence, and enhanced transport in accretion disks. *Rev. Mod. Phys.* **70,** 1–53 (1998).
15. Barge, P. & Sommeria, J. Did planet formation begin inside persistent gaseous vortices? *Astron. Astrophys.* **295,** L1–L4 (1995).
16. Fromang, S. & Nelson, R. P. On the accumulation of solid bodies in global turbulent protoplanetary disc models. *Mon. Not. R. Astron. Soc.* **364,** L81–L85 (2005).
17. Rice, W. K. M., Lodato, G., Pringle, J. E., Armitage, P. J. & Bonnell, I. A. Planetesimal formation via fragmentation in self-gravitating protoplanetary discs. *Mon. Not. R. Astron. Soc.* **372,** L9–L13 (2006).
18. Cuzzi, J. N., Hogan, R. C., Paque, J. M. & Dobrovolskis, A. R. Size-selective concentration of chondrules and other small particles in protoplanetary nebula turbulence. *Astrophys. J.* **546,** 496–508 (2001).
19. Hockney, R. W. & Eastwood, J. W. *Computer Simulation Using Particles* (McGraw-Hill, New York, 1981).
20. Gammie, C. F. Nonlinear outcome of gravitational instability in cooling, gaseous disks. *Astrophys. J.* **553,** 174–183 (2001).
21. Gammie, C. F. Layered accretion in T Tauri disks. *Astrophys. J.* **457,** 355–362 (1996).
22. Tanga, P., Weidenschilling, S. J., Michel, P. & Richardson, D. C. Gravitational instability and clustering in a disk of planetesimals. *Astron. Astrophys.* **427,** 1105–1115 (2004).
23. Salo, H. Gravitational wakes in Saturn's rings. *Nature* **359,** 619–621 (1992).
24. Boss, A. P. Giant planet formation by gravitational instability. *Science* **276,** 1836–1839 (1997).
25. Mayer, L., Quinn, T., Wadsley, J. & Stadel, J. Formation of giant planets by fragmentation of protoplanetary disks. *Science* **298,** 1756–1759 (2002).
26. Weidenschilling, S. J. Can gravitational instability form planetesimals? *Icarus* **116,** 433–435 (1995).
27. Dullemond, C. P. & Dominik, C. Dust coagulation in protoplanetary disks: A rapid depletion of small grains. *Astron. Astrophys.* **434,** 971–986 (2005).
28. Weidenschilling, S. J. The origin of comets in the solar nebula: A unified model. *Icarus* **127,** 290–306 (1997).
29. Throop, H. B. & Bally, J. Can photoevaporation trigger planetesimal formation? *Astrophys. J.* **623,** L149–L152 (2005).
30. Haghighipour, N. & Boss, A. P. On pressure gradients and rapid migration of solids in a nonuniform solar nebula. *Astrophys. J.* **583,** 996–1003 (2003).

Supplementary Information is linked to the online version of the paper at www.nature.com/nature.

Acknowledgements This collaboration was made possible through the support of the Annette Kade Graduate Student Fellowship Program at the American Museum of Natural History. J.S.O. was supported by the US National Science Foundation, as was M.-M.M.L. in part. We thank J. Cuzzi for discussion about the role of cooling in the gravitational collapse.

Author Information Reprints and permissions information is available at www.nature.com/reprints. The authors declare no competing financial interests. Correspondence and requests for materials should be addressed to A.J. (johansen@mpia.de).